Journal of Physics: Conference Series

PAPER • OPEN ACCESS

The convergence rate of a polygonal finite element for Stokes flows on different mesh families

To cite this article: T Vu-Huu *et al* 2021 *J. Phys.: Conf. Ser.* **1777** 012065

The convergence rate of a polygonal finite element for Stokes flows on different mesh families

T Vu-Huu[1,6], C Le-Thanh[2], Sy Pham-Van[1], Q Hoan Pham[1], H Nguyen-Xuan[3,4] and M Abdel-Wahab[5]

[1]Faculty of Civil Engineering, Vietnam Maritime University, Vietnam
[2]Faculty of Civil Engineering and Electricity, Ho Chi Minh City Open University, Vietnam
[3]CIRTech Institute, Ho Chi Minh City University of Technology (HUTECH), Ho Chi Minh City, Vietnam
[4]Department of Architectural Engineering, Sejong University, 209 Neungdong-ro, Gwangjin-gu, Seoul 05006, Republic of Korea
[5]Soete Laboratory, Faculty of Engineering and Architecture, Ghent University, Belgium

Email: truongvh.ctt@vimaru.edu.vn; magd.abdelwahab@ugent.be.

Abstract. This paper introduces an evaluation to consider the convergence rate of a polygonal finite element (PFE) to solve two-dimensional (2D) incompressible steady Stokes flows on different mesh families. For this purpose, a numerical example of 2D incompressible steady Stokes flows programmed and coded by MATLAB is deployed. Furthermore, the mixed equal-order PFE, i.e., Pe_1Pe_1, is utilised for this research. Additionally, five different mesh families, i.e., triangular, quadrilateral, hexagonal, random Voronoi, centroidal Voronoi meshes, are applied for this research. Moreover, an interesting evaluation of the CPU time for the performance of our proposed PFE in this research is employed as well. From these tests, differences in convergence rate, as well as CPU time of using Pe_1Pe_1 on different mesh families, are indicated.

Keywords: Fluid flow computations, polygonal finite elements, Stokes equations, convergence rate, mixed-method.

1. Introduction

Nowadays, among many potential numerical methods, e.g., finite volume method, smooth particle hydrodynamics, finite difference method, or finite element method (see Refs. [1-4]); polygonal finite element method (PFEM) is emerging as the most interesting method for fluid flow computations because of its special benefits in the good accuracy and high flexibility. Notably, it can be performed on almost mesh families, i.e., triangular, quadrilateral, random Voronoi mesh, etc. Additionally, this method has a desirable advantage of applying the properties of Voronoi diagrams mesh generation algorithms of arbitrary polygonal meshes [5, 6]. Moreover, one of the PFEM's advantages is the better accuracy comparing to the quadrilateral and triangular counterparts without the high request of the overall mesh size [7-9]. Furthermore, this research applies the study of Wachspress [10-12] to generate the polygonal basis shape functions for equal-order polygonal finite element, Pe_1Pe_1. Besides, to deal with a significant bottleneck of mesh quality in using PFEM, the advanced techniques proposed in Ref. [6] are applied.

In recent years, several interesting researches successfully proposed new PFEs for fluid flow computations. Particularly, Talischi et al. introduce a low-order mixed PFE, Pe_1Pe_0, in 2014 [13]. Then, in 2019, T. Vu-Huu et al. proposed two new polygonal finite elements, i.e., the equal-order polygonal finite element, Pe_1Pe_1, [14, 15] and a high-order polygonal finite element, MINIPe [16]. The proposed elements of T. Vu-Huu et al. accept the performance on all kinds of mesh families, e.g., triangular, quadrilateral, hexagonal, random Voronoi (RV), centroidal Voronoi (CVT) meshes instead of only hexagonal, RV and CVT mesh of Pe_1Pe_0. Therefore, this research is to evaluate the differences in convergence rates of Pe_1Pe_1 on five different mesh families. For this purpose, three kinds of error norms, i.e., the error of velocity, $e_{\mathbf{u}}^{L^2}$, error of pressure, $e_p^{L^2}$, in the approximation space L^2-norm and the velocity gradient error, $e_u^{H^1}$, in the approximation space H^1-norm are deployed to assess the convergence rate of Pe_1Pe_1. Finally, another interested evaluation of the CPU time of the proposed PFE is executed as well. For this aim, simulations with the similar of numbers of elements and the same of total degree freedoms (DOFs) are created to consider the difference of CPU time of Pe_1Pe_1 on the five different mesh families.

This paper is set up as follows: the governing Stokes equations of incompressible steady flows are presented in Section 2. Then, Section 3 briefly shows the polygonal discretisation system of the Stokes equations. Section 4 presents the results and discussions of the numerical test. Finally, Section 5. reports the conclusions.

2. Stoke governing equation system

The strong form of the Stokes equations for incompressible steady flows is [17]:

$$\nabla p - \nu\nabla^2\mathbf{u} = \mathbf{0} \quad \text{in } \Omega, \tag{1}$$

$$\nabla \cdot \mathbf{u} = 0 \tag{2}$$

In which modified pressure (after dividing by water density ρ) is denoted by p; fluid velocity is $\mathbf{u}$, and the constant positive kinematic viscosity is ν. Then, on the boundary, $\Gamma\Omega$, including the Dirichlet boundary, $\Gamma\Omega^D$, and the Neumann boundary, $\Gamma\Omega^N$, the boundary conditions are as follow:

$$\mathbf{u} = \mathbf{w} \quad \text{on } \Gamma\Omega^D, \tag{3}$$

$$\nu\frac{\partial\mathbf{u}}{\partial n} - \mathbf{n}p = \mathbf{s} \quad \text{on } \Gamma\Omega^N, \tag{4}$$

In which the outward-pointing normal is denoted by $\mathbf{n}$. Then, $\partial\mathbf{u}/\partial n$ denotes the derivative in the normal direction. The weak form of Eqs. (1)-(4) becomes:

$$\int_\Omega \mathbf{v}\cdot(-\nu\nabla^2\mathbf{u} + \nabla p)\mathrm{d}\Omega = 0 \quad \forall\, \mathbf{v} \in \mathbf{H}_0^1(\Omega), \tag{5}$$

$$\int_\Omega q\nabla\cdot\mathbf{u}\mathrm{d}\Omega = 0 \quad \forall\, q \in L_0^2(\Omega), \tag{6}$$

where $\mathbf{v}$ and q are the basis shape functions representing for velocity and pressure, respectively. Hence, the weak form becomes:

$$\nu\int_\Omega \nabla\mathbf{u}\colon\nabla\mathbf{v}\mathrm{d}\Omega - \int_\Omega p(\nabla\cdot\mathbf{v})\mathrm{d}\Omega = \int_{\Gamma\Omega^N}\mathbf{s}\cdot\mathbf{v}\mathrm{d}\Gamma\Omega, \tag{7}$$

$$\int_\Omega q(\nabla\cdot\mathbf{u})\,\mathrm{d}\Omega = 0, \tag{8}$$

in which the diffusion and convection term are denoted by $\nu\int_\Omega \nabla\mathbf{u}:\nabla\mathbf{v}\mathrm{d}\Omega$ and $\int_\Omega(\mathbf{u}\cdot\nabla\mathbf{u})\cdot\mathbf{v}\mathrm{d}\Omega$, respectively.

3. Polygonal discretisation system

In this research, the equal-order mixed PFE, i.e. Pe_1Pe_1, is applied by a similar set of basis functions for both velocity $\{\boldsymbol{\phi}_j\}$ and pressure field $\{\psi_k\}$ as follows:

$$\mathbf{u}_h = \sum_{j=1}^{n_u} \mathbf{u}_j \boldsymbol{\phi}_j + \sum_{j=n_u+1}^{n_u+n_\Gamma} \mathbf{u}_j \boldsymbol{\phi}_j, \tag{9}$$

$$p_h = \sum_{k=1}^{n_p} \mathbf{p}_k \psi_k, \tag{10}$$

where $\sum_{j=1}^{n_u} u_j \phi_j \in \mathbf{X}_0^h$. Then, the DOFs $\mathbf{u}_j : j = n_u + 1, \ldots, n_u + n_\Gamma$ is set for the second term on $\Gamma\Omega^D$.

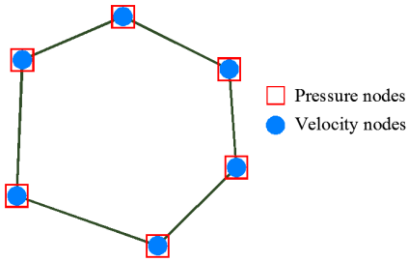

Figure 1. The mixed equal-order PFE: Pe_1Pe_1 [7, 16, 18-20].

In this research, the test functions, i.e. $\{\boldsymbol{\phi}_j\}$ and $\{\psi_k\}$ are the product of the set of Wachspress shape functions of an arbitrary interior point $\mathbf{v} \in \Omega^e$ as [6]:

$$\phi_i^e = \frac{\varphi_i}{\sum_{j=1}^{n_{ne}} \varphi_j} = \frac{\varphi_i}{\psi} \quad \text{with} \quad \varphi_i = \frac{S(\mathbf{x}_{i-1}, \mathbf{x}_i, \mathbf{x}_{i+1})}{S(\mathbf{v}, \mathbf{x}_{i-1}, \mathbf{x}_i) S(\mathbf{v}, \mathbf{x}_i, \mathbf{x}_{i+1})} \tag{11}$$

where the area of the triangle $[\mathbf{x}_a, \mathbf{x}_b, \mathbf{x}_c]$ is $S(\mathbf{x}_a, \mathbf{x}_b, \mathbf{x}_c)$, see Figure 2. (a).

In addition, an adaption is the perpendicular Wachspress coordinates of the distances, $h_i(\mathbf{x})$, between point $\mathbf{v}$ and sides of Ω^e (see Figure 2 (b)). Then, the $\mathbf{p}_i(\mathbf{x})$ is the ratio between $\mathbf{n}_i$ (the outward unit normal vector) and the distance $h_i(\mathbf{x})$ to the side $\mathbf{e}_i = [\mathbf{x}_i, \mathbf{x}_{i+1}]$ of an element with vertices indexed cyclically $\mathbf{x}_{n+1} = \mathbf{x}_1$.

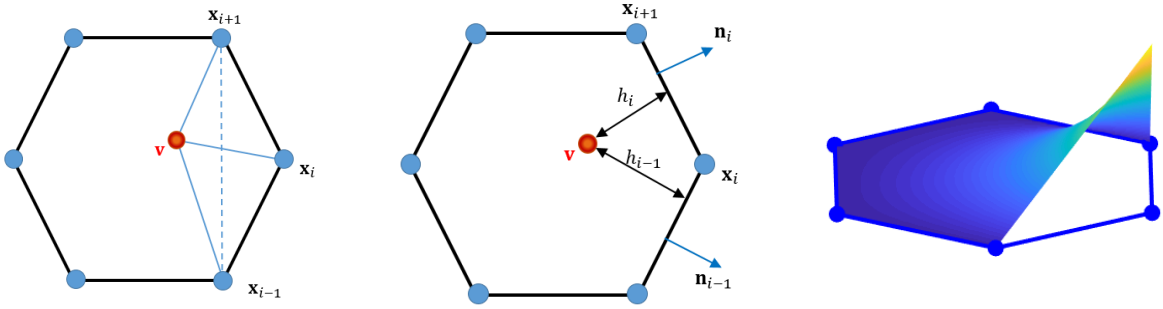

(a) (b) (c)

Figure 2. Sample of Wachspress shape functions on a hexagonal element: a) Triangles definition, b) Perpendicular distances, c) 3D representative sample [11, 12, 21].

Then, the polygonal shape functions based on the Wachspress definition become:

$$\phi_i^e = \frac{\varphi_i}{\varphi} = \frac{\tilde{\varphi}_i}{\sum_{j=1}^{n_{ne}} \tilde{\varphi}_i} \text{ with } \tilde{\varphi}_i = det(\mathbf{p}_{i-1}, \mathbf{p}_i) \tag{12}$$

and their gradients are:

$$\nabla\phi_i^e = \phi_i^e\left[\vartheta_i - \sum\nolimits_{j=1}^{n_{ne}} \phi_j^e \vartheta_j\right] \text{ where } \vartheta_i = \mathbf{p}_{i-1} + \mathbf{p}_i. \tag{13}$$

Because of using the equal-order mixed PFE, Pe_1Pe_1, causes instability problem, a special treatment introduced in Refs. [16, 18-20] is applied to eliminate the instability problem of Pe_1Pe_1. For this technique, the local stabilisation matrix of a polygonal finite element with n_{ne} c_e is:

$$\begin{aligned} c_e(p_h, q_h) &= \int_{\Omega_e} (p_h - \prod p_h)(q_h - \prod q_h)\,\mathrm{d}\Omega \\ &= \sum_{i,j=1}^{n_{ne}} q_i \int_{\Omega_e} \left(\psi_i - \frac{1}{n_{ne}}\right)\left(\psi_j - \frac{1}{n_{ne}}\right)\mathrm{d}\Omega\; q_j \qquad \forall\Omega_e \in \Im_h, \end{aligned} \tag{14}$$

where the indices i and j of the basis functions ψ_i and ψ_j is get values on the element Ω_e. Then, the global stabilization matrix $\mathbf{C}$ for polygonal mesh is:

$$\mathbf{C} = \mathop{\mathbf{A}}_{e=1}^{n_e} \sum_{i,j=1}^{n_{ne}} \int_{\Omega_e} \left(\psi_i - \frac{1}{n_{ne}}\right)\left(\psi_j - \frac{1}{n_{ne}}\right)\mathrm{d}\Omega, \tag{15}$$

Finally, the discretisation Stokes system Eqs. (7) - (8) becomes:

$$\begin{bmatrix} \mathbf{A} & \mathbf{B}^T \\ \mathbf{B} & -\mathbf{C} \end{bmatrix} \begin{bmatrix} \mathbf{u} \\ \mathbf{p} \end{bmatrix} = \begin{bmatrix} \mathbf{f} \\ \mathbf{g} \end{bmatrix}. \tag{16}$$

In which, the vector-Laplacian $\mathbf{A}$ is:

$$\mathbf{A} = [\mathbf{a}_{ij}], \quad \mathbf{a}_{ij} = \int_{\Omega} \nabla\boldsymbol{\phi}_i : \nabla\boldsymbol{\phi}_j \mathrm{d}\Omega, \tag{17}$$

Then, the divergence matrix $\mathbf{B}$ is:

$$\mathbf{B} = [b_{kj}], \quad b_{kj} = -\int_{\Omega} \psi_k \nabla . \boldsymbol{\phi}_j \mathrm{d}\Omega, \tag{18}$$

with $k = 1, \ldots, n_p$; i and $j = 1, \ldots, n_u$. Additionally, the right-hand side terms are defined as:

$$\mathbf{f} = [\mathbf{f}_i], \quad \mathbf{f}_i = \int_{\Gamma\Omega^N} \mathbf{s} . \boldsymbol{\phi}_i \mathrm{d}\Gamma\Omega - \sum_{j=n_u+1}^{n_u+n_\Gamma} \mathbf{u}_j \int_{\Omega} \nabla\boldsymbol{\phi}_i : \nabla\boldsymbol{\phi}_j \mathrm{d}\Omega, \tag{19}$$

$$\mathbf{g} = [\mathbf{g}_k], \quad \mathbf{g}_k = \sum_{j=n_u+1}^{n_u+n_\Gamma} \mathbf{u}_j \int_{\Omega} \psi_k \nabla . \boldsymbol{\phi}_j \mathrm{d}\Omega. \tag{20}$$

4. Numerical tests

In this research, a numerical example showing the incompressible steady Stokes flow is applied to evaluate the accuracy of the equal-order PFE on different mesh families. This example shows a two dimensional (2D) laminar flow in a standard square domain $\Omega = (-1,1)^2$. For this test, the following conditions are deployed: (1) the kinematic viscosity is set by one on the whole domain; (2) the velocities on top ($y = 1$) and bottom ($y = -1$) of the boundary are set to zero; (3) the inflow is set as $u_x = 1 - y^2$ and $u_y = 0$ at $x = -1$; and (4) the outflow is controlled by a natural boundary condition at $x = 1$ and $-1 < y < 1$, as follows:

$$\begin{aligned} -p + \frac{\partial u_x}{\partial x} &= 0, \\ \frac{\partial u_y}{\partial x} &= 0. \end{aligned} \tag{21}$$

This test is generally called Poiseuille flow - an exact solution of the Navier–Stokes (N-S) problems. For more discussions, readers can refer to Refs. [16, 18-20, 22]. In this paper, three error norms are applied to assess the accuracy as well as the convergence rate of Pe_1Pe_1 [15, 23]:

$$e_u^{L^2} = \|\mathbf{u}_0 - \mathbf{u}_h\|_0 = \left(\sum_{i=1}^{n_e} \int_{\Omega_e} (\mathbf{u}_0 - \mathbf{u}_h)\,(\mathbf{u}_0 - \mathbf{u}_h) \mathrm{d}\Omega \right)^{\frac{1}{2}}, \tag{22}$$

$$e_u^{H^1} = \|\mathbf{u}_0 - \mathbf{u}_h\|_1 = \left(\sum_{i=1}^{n_e} \int_{\Omega_e} (\nabla\mathbf{u}_0 - \nabla\mathbf{u}_h).(\nabla\mathbf{u}_0 - \nabla\mathbf{u}_h) \mathrm{d}\Omega \right)^{\frac{1}{2}}, \tag{23}$$

$$e_p^{L^2} = \|p_0 - p_h\|_0 = \left(\sum_{i=1}^{n_e} \int_{\Omega_e} (p_0 - p_h)\,(p_0 - p_h) \mathrm{d}\Omega \right)^{\frac{1}{2}}, \tag{24}$$

in which $(\mathbf{u}_h, p_h)$ and $(\mathbf{u}_0, p_0)$ respectively are the approximation and exact solutions. Then, $e_{\mathbf{u}}^{L^2}$ and $e_p^{L^2}$ are the error of velocity and pressure in L^2-norm, respectively. Besides, $e_u^{H^1}$ is the velocity gradient error in H^1-norm. Moreover, five mesh families (see Figure 3) are generated for this test:

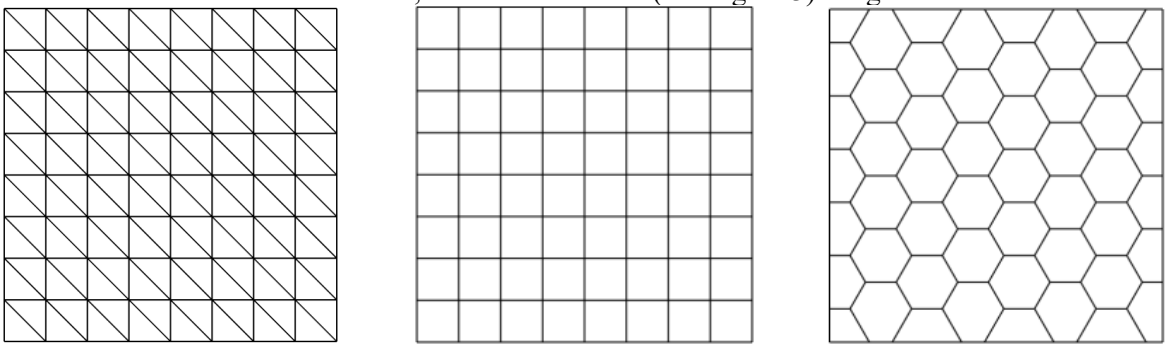

(a) Triangular mesh. (b) Quadrilateral mesh. (c) Hexagonal mesh.

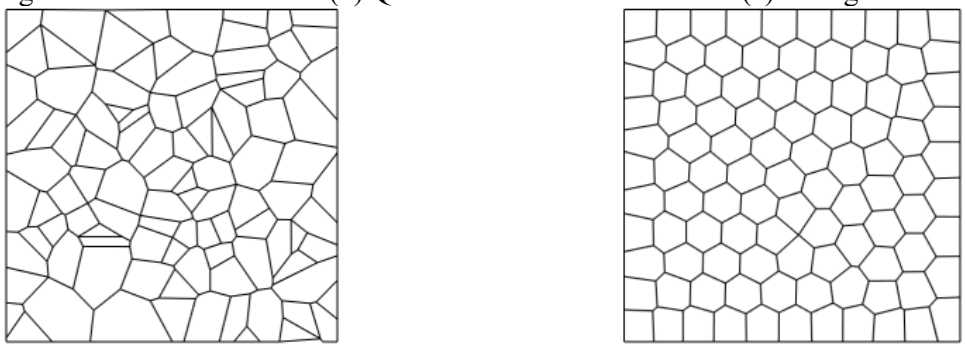

(d) Random Voronoi mesh (RV). (e) Centroid Voronoi mesh (CV).

Figure 3. Five samples of polygonal mesh families [16, 18-20].

The results of this test are firstly presented in Figure 4 that show the error norms of velocity, velocity gradient, pressure fields on five different mesh families. Additionally, for each mesh family, the computation is employed on seven progressively finer meshes to assess the convergence rate of the current technique. The results of error norms presented in Figure 4 shows the accuracy that is the function of mesh size h. All convergence rates are close to the optimal values of the respective error norms. Even the convergence rate of pressure is faster than the expected convergence rate. For example, the convergence rate of pressure on triangular and quadrilateral meshes is 1.8, and on hexagonal, CV, RV meshes is 1.2. Moreover, the next results of convergence rates of this test are shown in Figure 5, which is the function of DOFs.

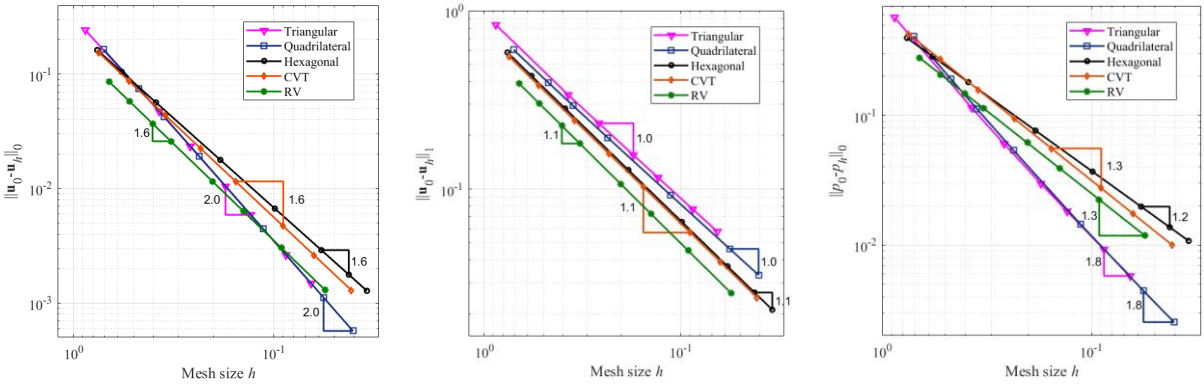

(a) $e_{\boldsymbol{u}}^{L^2}$ − error norm of velocity. (b) $e_{\boldsymbol{u}}^{H^1}$ − error norm of velocity gradient. (c) $e_p^{L^2}$ − error norm of pressure.

Figure 4. Errors versus mesh size h of Pe_1Pe_1 (the horizontal axis is set reversely).

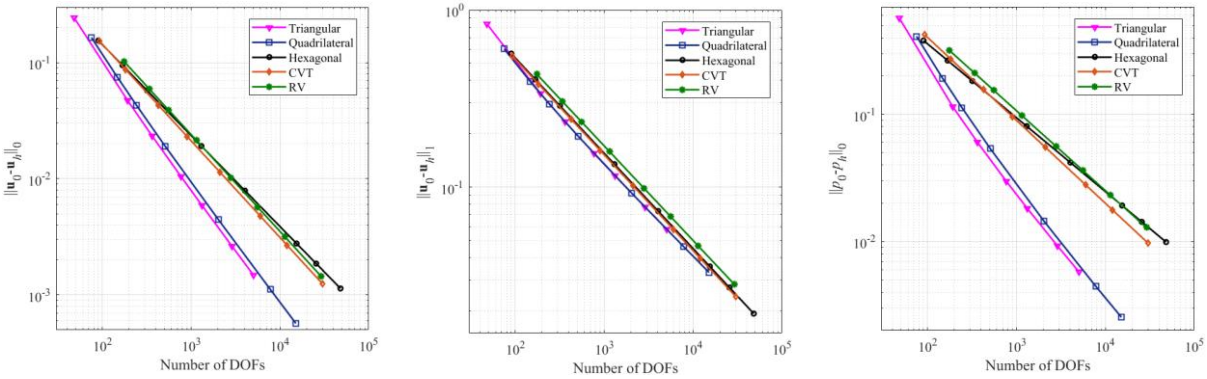

(a) $e_{\boldsymbol{u}}^{L^2}$ − error norm of velocity. (b) $e_{\boldsymbol{u}}^{H^1}$ − error norm of velocity gradient. (c) $e_p^{L^2}$ − error norm of pressure.

Figure 5. Errors versus DOFs of Pe_1Pe_1.

As Figure 4 and Figure 5 of this test, they show a trend of the better convergence rate in the triangular and quadrilateral mesh. Particularly, both mesh families provide similar convergence rates, i.e., 2.0 for velocity, 1.8 for pressure. However, because this example is only tested on a standard square domain with a horizontal laminar Stokes flow, the result could be different in the tests of more complicated domains and flows.

The next aim of this research is to consider the CPU time of Pe_1Pe_1 for this test in the five different mesh families at a similar number of DOFs and the same numbers of elements, respectively, see Chapter 11.1a.Fig. 1.Table 1 and 0.

Table 1. CPU time on different mesh families with the similar DOFs.

Mesh	No. Elements	No. Nodes	DOFs	CPU Time (s)
Triangular	9800	5041	15123	34.5032
Quadrilateral	4900	5041	15123	20.4431
Hexagonal	2565	5132	15369	19.6857
RV	2600	5031	15093	18.5640
CV	2550	5101	15303	18.9633

As seen in Table 1, which shows the CPU time at similar DOFs, it is clear that triangular mesh need the highest CPU time for computations, then quadrilateral mesh and the other ones, e.g. hexagonal, RV, and CV. It causes by the much higher numbers of elements on triangular and

quadrilateral meshes than the others, e.g. hexagonal, CV, RV. As known, the computational cost depends on the number of Gauss points of the quadrature rule; the greater number of elements of triangular mesh leads to the higher CPU time. Furthermore, another noticeable thing in Table 1 is the not much difference of CPU time between quadrilateral mesh with the other ones, e.g. hexagonal, RV and CV, even the numbers of elements of quadrilateral mesh is double of hexagonal, RV and CV. Therefore, to have a deeper evaluation of this perspective, the comparison of CPU time on different mesh families with the similar numbers of elements is provided in Table 2 as follows.

Table 2. CPU time on different mesh families with the similar numbers of elements.

Mesh	No. Elements	No. Nodes	DOFs	CPU Time (s)
Triangular	5000	2601	7803	13.9138
Quadrilateral	5041	5184	15552	29.0871
Hexagonal	5092	10186	30558	46.5223
RV	5000	9595	28785	46.8393
CV	5000	10001	30003	48.2422

As see in Table 2, now we see the highest CPU time on the hexagonal, RV, CV mesh. As mentioned before, the computational cost depends on the number of Gauss points of the quadrature rule. In this research, because of using the technique introduced in Refs. [24, 25], the number of Gauss points on the triangle and quadrilateral is lowest. In conclusion, we can see that at the same of numbers of elements, the mesh of triangles spends less CPU time than the other of mesh families. Meanwhile, with the same numbers of DOFs, the triangular mesh needs the highest CPU time for computations.

5. Conclusion

In this research, an evaluation to present differences in the convergence rate as well as CPU time of an equal-order PFE on five different mesh families. This research bases on the mixed equal-order scheme on polygons, Pe_1Pe_1 [18, 19]. As this research, we can see that the better in accuracy and convergence rates of Pe_1Pe_1 on the triangular and quadrilateral mesh. Particularly, the results on triangular and quadrilateral meshes provide faster convergence rates than the other mesh families, e.g., hexagonal mesh, RV, CVT. Moreover, as the tests of CPU time in this research, with the same of DOFs, the triangular mesh needs more CPU time than the other mesh families. In addition, for the same numbers of elements, the triangular mesh needs the lowest CPU time for computations. However, because this research is limited to only one numerical example, this research could be extended with the other tests with more complex domains and complicated flows to get more general conclusions.

Acknowledgement

The authors acknowledge the financial support of VLIR-OUS TEAM Project, VN2017TEA454A103, 'An innovative solution to protect Vietnamese coastal riverbanks from floods and erosion'.

References

[1] Chung T 2010 *Computational Fluid Dynamics* (Cambridge: Cambridge University Press)
[2] Ferziger J H and Perić M 2002 *Computational Methods for Fluid Dynamics* vol 3 (Springer)
[3] Donea J and Huerta A 2003 *Finite Element Methods for Flow Problems* (John Wiley & Sons)
[4] Liu G-R and Liu M B 2003 *Smoothed Particle Hydrodynamics: A Meshfree Particle Method* (World Scientific)
[5] Sieger D, Alliez P and Botsch M 2010 Optimizing Voronoi Diagrams for Polygonal Finite Element Computations *Proc. the 19th Int. Meshing Roundtable* (Berlin: Springer) pp 335-50

[6] Talischi C, Paulino G H, Pereira A and Menezes I F 2012 PolyMesher: a general-purpose mesh generator for polygonal elements written in Matlab *Struct. Multidiscip. O* **45** 309-28
[7] Vu-Huu T, Le-Thanh C, Nguyen-Xuan H and Wahab M A 2018 Incompressible Fluid Computation Based on Polygonal Finite Element. *Int. Conf. on Numerical Modelling in Engineering* 202-12
[8] Vu-Huu T, Phung-Van P, Nguyen-Xuan H and Wahab M A 2018 A polytree-based adaptive polygonal finite element method for topology optimization of fluid-submerged breakwater interaction *Comput. Math. Appl.* **76** 1198-218
[9] Vu-Huu T, Le-Thanh C, Phung-Van P, Nguyen-Xuan H and Abdel-Wahab M 2017 Fluid–Structure Interaction Analysis of Revetment Structures—An Overview *Int. Conf. on Advances in Computational Mechanics* 723-31
[10] Wachspress E L 1975 *A Rational Finite Element Basis* (Elsevier)
[11] Floater M S 2014 Wachspress and mean value coordinates. In: *Approximation Theory XIV: San Antonio 2013* pp 81-102
[12] Floater M, Gillette A and Sukumar N 2014 Gradient bounds for Wachspress coordinates on polytopes *SIAM J. Numer. Anal.* **52** 515-32
[13] Talischi C, Pereira A, Paulino G H, Menezes I F and Carvalho M S 2014 Polygonal finite elements for incompressible fluid flow *Int. J. Numer. Meth. Fl.* **74** 134-51
[14] Bathe K-J 2001 The inf–sup condition and its evaluation for mixed finite element methods *Comput. Struct.* **79** 243-52
[15] Dohrmann C R and Bochev P B 2004 A stabilized finite element method for the Stokes problem based on polynomial pressure projections *Int. J. Numer. Meth. Fl.* **46** 183-201
[16] Vu-Huu T, Le-Thanh C, Nguyen-Xuan H and Abdel-Wahab M 2019 A high-order mixed polygonal finite element for incompressible Stokes flow analysis *Comput. Method Appl. M.* **356** 175-98
[17] Elman H C, Silvester D J and Wathen A J 2014 Finite elements and fast iterative solvers: with applications in incompressible fluid dynamics *Numer. Math. Sci. Comp.*1595-96
[18] Vu H T, Le T C, Nguyen-Xuan H and Abdel Wahab M 2020 Stabilization for Equal-Order Polygonal Finite Element Method for High Fluid Velocity and Pressure Gradient *CMC-Computers, Materials & Continua* **62** 1109-23
[19] Vu-Huu T, Le-Thanh C, Nguyen-Xuan H and Wahab M A 2020 Equal-order polygonal analysis for fluid computation in curved domain *Int. J. Comput. Methods*
[20] Vu-Huu T, Le-Thanh C, Nguyen-Xuan H and Abdel-Wahab M 2020 An equal-order mixed polygonal finite element for two-dimensional incompressible Stokes flows *Eur. J. Mech. B-Fluid* **79** 92-108
[21] Chau K N, Chau K N, Ngo T, Hackl K and Nguyen-Xuan H 2018 A polytree-based adaptive polygonal finite element method for multi-material topology optimization *Comput. Method Appl. M.* **332** 712-39
[22] Callaghan P T 2011 *Translational Dynamics and Magnetic Resonance:Principles of Pulsed Gradient Spin Echo NMR* (Oxford University Press)
[23] Bochev P B, Dohrmann C R and Gunzburger M D 2006 Stabilization of low-order mixed finite elements for the Stokes equations *SIAM J. Numer. Anal.* **44** 82-101
[24] Sukumar N 2004 Construction of polygonal interpolants: a maximum entropy approach *International Int. J. Numer. Meth. Eng.* **61** 2159-81
[25] Sukumar N and Tabarraei A 2004 Conforming polygonal finite elements *Int. J. Numer. Meth. Eng.* **61** 2045-66